



MOX-Report No. 44/2021

**Efficient Modeling of Multimode Guided Acoustic Wave  
Propagation in Deformed Pipelines by Hierarchical  
Model Reduction**

Gentili, G.G.; Khosronejad, M.; Bernasconi, G.; Perotto, S.;  
Micheletti, S.

MOX, Dipartimento di Matematica  
Politecnico di Milano, Via Bonardi 9 - 20133 Milano (Italy)

[mox-dmat@polimi.it](mailto:mox-dmat@polimi.it)

<http://mox.polimi.it>

# Efficient Modeling of Multimode Guided Acoustic Wave Propagation in Deformed Pipelines by Hierarchical Model Reduction

G.G. Gentili<sup>†</sup>, M. Khosronejad<sup>†</sup>, G. Bernasconi<sup>†</sup>,  
S. Perotto<sup>#</sup>, S. Micheletti<sup>#</sup>

June 30, 2021

<sup>†</sup> Dipartimento di Elettronica, Informazione e Bioingegneria  
Politecnico di Milano, P.zza L. da Vinci 32, I-20133 Milano, Italy  
{gianguido.gentili,misagh.khosronejad,giancarlo.bernasconi}@polimi.it

<sup>#</sup> MOX – Modellistica e Calcolo Scientifico, Dipartimento di Matematica  
Politecnico di Milano, Piazza L. da Vinci 32, I-20133 Milano, Italy  
{simona.perotto,stefano.micheletti}@polimi.it

## Abstract

The finite element based hierarchical model (HiMod) reduction technique is here applied, for the first time, to model guided acoustic wave propagation in deformed pipelines in a linear regime. This method turns out to be extremely efficient to discretize the linearized Helmholtz equation for acoustic waves. The selection of a suitable modal transverse basis for the acoustic field allows us to speed up the computation by orders of magnitude with respect to a standard 3D finite element discretization.

Keywords: Finite element method, acoustic waves, modal propagation, pipelines, hierarchical model reduction

## 1 Introduction

Reflectometric techniques based on guided acoustic waves in pipelines are well established non-destructive tools for monitoring the status of pipelines [1, 2, 3, 4]. Basically, concentrated or distributed reflections are caused by a change in the local cross-section area of the pipeline as a result of deformation [5, 6]. These reflections provide useful information about the shape, the level and the position of deformations along the pipeline. Reflectometric techniques are almost always based on single mode propagation, when only the main mode, having uniform pressure over the pipe transverse cross-section, propagates. In these cases, a very efficient and rather accurate description of the scattering problem can be obtained by modeling the wave in the pipeline in one-dimension

(1D) [5]. However, there are some limitations to this approach: first, the usable bandwidth of analysis is limited to that of single mode propagation and, depending on the size of the pipeline, this can be a rather severe constraint; secondly, higher order modes scattering coefficients are not available, although the amount of information contained in these coefficients is very rich and useful. The actual reason why single-mode propagation is considered is the high computational demand for a multimode scattering analysis in arbitrarily deformed pipelines. Such computational task requires a discretization based on three-dimensional (3D) Finite Elements (FE) or Finite Differences (FD), which are very demanding in terms of CPU time and storage. As for FE and FD methods, there is a clear superiority of FE since they allow a more accurate description of the geometry. Actually, unless some very special geometry is considered, FD require an extremely fine discretization of curved shapes, making it often non-competitive with respect to 3D FE. Moreover, we also mention that FE rely on a sound theoretical background based on functional analysis and calculus of variations topics. Even so, full 3D FE for linear acoustic propagation can become very challenging according to the size of the domain and the bandwidth of analysis, the mesh size being dependent on the maximum frequency of interest [7].

In this work, we address the problem of modeling multimode acoustic scattering in deformed pipelines by an ad-hoc FE discretization based on the Hierarchical Model (HiMod) reduction technique. This reduction procedure proved to be an extremely efficient and powerful tool in haemodynamic modeling, by allowing accurate patient-specific simulations with a considerable reduction in terms of CPU time [8]. The main strength of the HiMod approach is the capability to include in the modeling the transverse dynamics which are usually discarded by purely 1D models, while solving problems defined in a 1D domain. HiMod reduction exploits the idea of coupling separation of variables with different numerical approximations, to take advantage of an intrinsic directionality of the problem at hand. In the original proposal, HiMod discretization employs FE to discretize the mainstream, while a suitable modal expansion models the transverse components [9, 10, 11]. More recently, in [12] the authors enhanced the discretization along the leading direction by resorting to an isogeometric approximation, setting the isogeometric version of the HiMod procedure, known as HIgaMod reduction. The fast convergence of spectral approximations ensures to detect the main features of the transverse dynamics with a relatively low number of modes. This turns out into an accurate approximation with a contained number of degrees of freedom (dofs) when compared with a non-customized modeling such as classical 3D FE solvers.

HiMod reduction massively exploits a transformation of coordinates (the HiMod map) that changes the physical into a reference domain, namely the pipeline into a straight undeformed tube. An exact equivalence between the original problem (defined in the deformed pipeline) and the new one (defined in the undeformed domain) is established by introducing an artificial anisotropic material, whose characteristic parameters are identified by the HiMod map itself. In the acoustics literature, the coordinate transformation technique is often referred to as Transformation Acoustics [13, 14]. The identification of a suitable map represents a key step of the whole procedure presented in this pa-

per. This is consistent with a HiMod discretization, whose main effort is represented by the identification of the HiMod map, together with the definition of the modal basis [15, 16, 17, 8].

The paper is organized as follows. In Section 2, we recall how a coordinate transformation affects the linearized acoustic wave equation. In Section 3, we introduce the weak form for linearized acoustic waves and the standard FE discretization in the general case of materials with anisotropic density. In Section 4, we discuss the HiMod discretization according to which the transverse and longitudinal dynamics are expressed by separation of variables. In Section 5, we define the multimode acoustic impedance matrix, the multimode acoustic scattering matrix, and their mutual relationships. The coefficients of the scattering matrix provide the parameters that we use to compare HiMod with well-established techniques based on FE. Comparison results are shown in Section 6, where we provide a set of examples for verification, together with a discussion on the numerical performance of the method proposed in this paper. In Section 7, we draw some conclusions and present possible future developments. Finally, in Appendix A, we present the specific coordinate transformation that we used to convert a generic deformed pipeline into an undeformed one, while in Appendix B we provide the full expression for the acoustic modal functions used in the HiMod reduction.

## 2 Coordinate transformation and the transformed wave model

A HiMod discretization can be conceptually split into two phases [9, 10, 11]. The first step consists in defining a coordinate transformation that changes the pipeline into a constant cross-section tube; as a second step, the unknown function (in our case, the pressure field in the Helmholtz equation) is expanded in terms of 1D FE, which discretize the direction of propagation, and of modal functions, which describe the transverse dynamics over the pipe cross-section.

In this section, we focus on the HiMod map and we describe how the coordinate transformation affects the wave equation. Then, we define the pressure field to be expanded via a HiMod discretization for the configuration of utmost interest in practical applications, i.e., for a circular cross-section pipeline endowed with two ports located at the end points of the pipe. The two ports act, alternatively, as source or receiver.

The problem is originally defined in a pipeline characterized by a deformed circular cross-section in the framework of coordinates  $x'$ ,  $y'$ ,  $z'$  (see Figure 1). In particular, we denote by  $\Omega'$  the domain of analysis and by  $\partial\Omega'$  the corresponding boundary. Letting  $\psi' = \psi'(x', y', z')$  the pressure field, the linearized acoustic wave equation in the frequency domain is obtained by exploiting Euler's equation

$$\nabla' \psi' = -j\omega \rho_0 \vec{v}', \quad (1)$$

and the continuity equation

$$j\omega \psi' = -b_0 \nabla' \cdot \vec{v}', \quad (2)$$

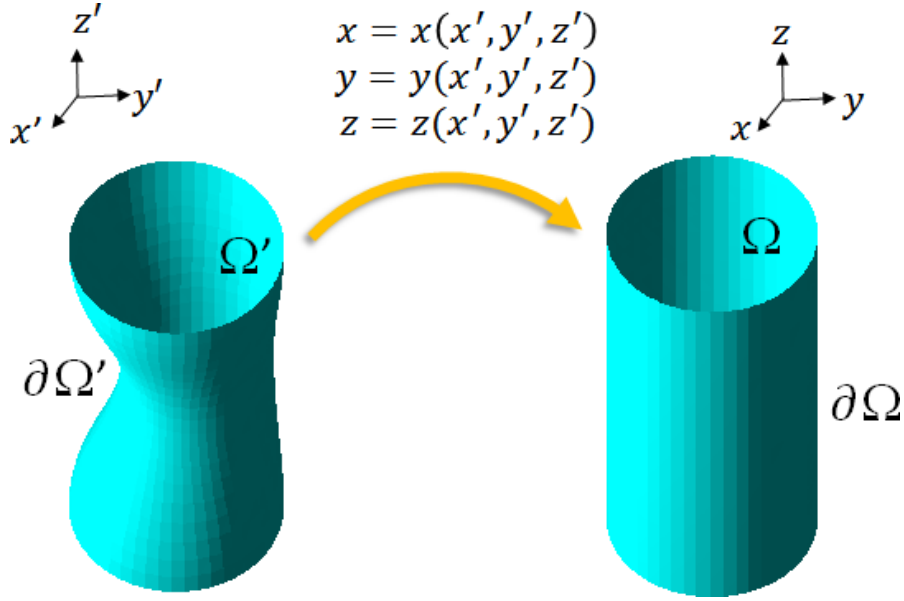


Figure 1: The HiMod map transforming a deformed cylinder to a constant cross-section cylinder.

where  $\varrho_0$  is the rest density,  $b_0$  is the compression modulus,  $\bar{v}'$  is the particle speed,  $\omega$  is the wave angular frequency and  $j$  denotes the imaginary unit. In (1)-(2), we have dropped the standard time dependence,  $e^{j\omega t}$ , since we operate in the Fourier transform domain [5, 18]. By substitution of (2) into (1) and adding suitable boundary conditions, we obtain the well-known linearized acoustic wave equation

$$\begin{cases} \nabla' \cdot (\nabla' \psi') + k_0^2 \psi' = 0 & \text{in } \Omega' \\ \nabla' \psi' \cdot \nu' = F & \text{on } \partial\Omega', \end{cases} \quad (3)$$

where  $k_0 = \omega \sqrt{\varrho_0/b_0}$  is the wavenumber,  $\nu'$  is the unit inward normal vector to the boundary, and  $F$  is a given function modeling an impressed normal speed of the particles on the boundary  $\partial\Omega'$ .

Now, we change the reference framework and we consider the new setting

$$\begin{cases} x = x(x', y', z') \\ y = y(x', y', z') \\ z = z', \end{cases} \quad (4)$$

so that the pipe  $\Omega'$  commutes into the new domain  $\Omega$ , whose boundary,  $\partial\Omega$ , is a perfectly circular cylinder with the same length,  $L$ , as the original structure (see Figure 1). As a consequence, the (unknown) pressure  $\psi'$  is replaced by the new field  $\psi(x, y, z)$ . It can be shown that  $\psi(x, y, z)$  and  $\psi'(x', y', z')$  do coincide at the corresponding points in the settings  $x, y, z$  and  $x', y', z'$ , if the Euler and the continuity equations are modified into

the following form

$$\frac{\overline{\overline{\mathbf{J}}}\overline{\overline{\mathbf{J}}}^T}{\det(\overline{\overline{\mathbf{J}}})}\nabla\psi = -j\omega\rho_0\bar{v}, \quad (5)$$

and

$$j\omega\psi = -b_0 \det(\overline{\overline{\mathbf{J}}}) \nabla \cdot \bar{v}, \quad (6)$$

respectively [19, 13, 20, 21], where  $\overline{\overline{\mathbf{J}}} = \overline{\overline{\mathbf{J}}}(x, y, z)$  is the second-rank tensor given by the matrix form

$$\overline{\overline{\mathbf{J}}} = \begin{bmatrix} \frac{\partial x}{\partial x'} & \frac{\partial x}{\partial y'} & \frac{\partial x}{\partial z'} \\ \frac{\partial y}{\partial x'} & \frac{\partial y}{\partial y'} & \frac{\partial y}{\partial z'} \\ \frac{\partial z}{\partial x'} & \frac{\partial z}{\partial y'} & \frac{\partial z}{\partial z'} \end{bmatrix} = \begin{bmatrix} \frac{\partial x}{\partial x'} & \frac{\partial x}{\partial y'} & \frac{\partial x}{\partial z'} \\ \frac{\partial y}{\partial x'} & \frac{\partial y}{\partial y'} & \frac{\partial y}{\partial z'} \\ 0 & 0 & 1 \end{bmatrix}, \quad (7)$$

where the simplification on the right-hand side is due to the assumption  $z' = z$ . Acoustic field manipulation by coordinate transformation is often referred to as Transformation Acoustics. Some applications are available in the literature (see, e.g., [13, 20, 21, 22, 14]). A cross comparison between (1)-(2) and (5)–(6) shows that the equivalence between  $\psi'$  and  $\psi$  can be obtained by replacing air with a material having an anisotropic relative density

$$\overline{\overline{\rho}}_r = \left[ \frac{\overline{\overline{\mathbf{J}}}\overline{\overline{\mathbf{J}}}^T}{\det(\overline{\overline{\mathbf{J}}})} \right]^{-1}.$$

Finally, by substitution of (6) into (5), we obtain the counterpart of problem (3) in the new reference framework, i.e., the transformed wave equation, given by

$$\nabla \cdot (\overline{\overline{\mathbf{T}}}\nabla\psi) + \frac{k_0^2}{\det(\overline{\overline{\mathbf{J}}})}\psi = 0 \quad \text{in } \Omega, \quad (8)$$

with boundary condition

$$(\overline{\overline{\mathbf{T}}}\nabla\psi) \cdot \nu = F \quad \text{on } \partial\Omega, \quad (9)$$

with  $\nu$  the unit inward normal vector to  $\partial\Omega$  and

$$\overline{\overline{\mathbf{T}}} = \overline{\overline{\rho}}_r^{-1} = \frac{\overline{\overline{\mathbf{J}}}\overline{\overline{\mathbf{J}}}^T}{\det(\overline{\overline{\mathbf{J}}})}$$

a symmetric second-rank tensor. The specific form of the transformation used in this work is provided in appendix A, together with the explicit expression of the elements of tensor  $\overline{\overline{\mathbf{J}}}$  (in polar coordinates).

### 3 A full finite element formulation

To provide the discrete counterpart of problem (8)-(9), we start from the associated weak form, which leads to looking for the pressure field  $\psi \in V = H^1(\Omega)$ , such that

$$\int_{\Omega} \nabla\varphi \cdot \overline{\overline{\mathbf{T}}}\nabla\psi \, d\Omega - k_0^2 \int_{\Omega} \frac{\varphi\psi}{\det(\overline{\overline{\mathbf{J}}})} \, d\Omega = \int_{\partial\Omega} \varphi (\overline{\overline{\mathbf{T}}}\nabla\psi) \cdot \nu \, dS \quad (10)$$

for any  $\varphi \in V$ , where  $H^1(\Omega)$  denotes the Sobolev space of the  $L^2(\Omega)$ -functions (i.e., the space of square integrable functions in  $\Omega$ ) with first order weak derivative in  $L^2(\Omega)$  [23]. By exploiting the boundary condition in (9), we look for  $\psi \in V$  such that

$$\int_{\Omega} \nabla \varphi \cdot \overline{\overline{T}} \nabla \psi \, d\Omega - k_0^2 \int_{\Omega} \frac{\varphi \psi}{\det(\overline{\overline{J}})} \, d\Omega = \int_{\partial\Omega} \varphi F \, dS \quad \forall \varphi \in V. \quad (11)$$

In the next sections, we will exploit the weak form (11) to define a representation of the scattering problem in terms of the so-called multimodal acoustic impedance matrix. With this goal, we apply the Galerkin method to (11) [23]. We introduce the discrete space  $V_h \subset V$ , with  $\dim(V_h) = N_h < +\infty$ , spanned by the basis functions in  $\mathcal{B} = \{\psi_q\}_{q=1}^{N_h}$ . Thus, the unknown pressure field  $\psi$  can be approximated via a function  $\tilde{\psi} \in V_h$ , coinciding with an expansion in terms of the basis  $\mathcal{B}$ , being

$$\tilde{\psi}(x, y, z) = \sum_{q=1}^{N_h} c_q \psi_q(x, y, z), \quad (12)$$

while the test function in (11) can be identified with  $\psi_p$ , with  $p = 1, \dots, N_h$ . The algebraic counterpart of the Galerkin approximation for problem (11) can be stated in a straightforward way as

$$(\mathbf{A} - k_0^2 \mathbf{B}) \mathbf{c} = \mathbf{d}, \quad (13)$$

where the matrices  $\mathbf{A}, \mathbf{B} \in \mathbb{R}^{N_h \times N_h}$ , and the vectors  $\mathbf{c}, \mathbf{d} \in \mathbb{C}^{N_h \times 1}$  are defined by

$$\begin{aligned} \mathbf{A}_{p,q} &= \int_{\Omega} \nabla \psi_p \cdot \overline{\overline{T}} \nabla \psi_q \, d\Omega, \\ \mathbf{B}_{p,q} &= \int_{\Omega} \frac{\psi_p \psi_q}{\det(\overline{\overline{J}})} \, d\Omega, \\ \mathbf{c}_{q,1} &= c_q, \\ \mathbf{d}_{p,1} &= \int_{\partial\Omega} \psi_p F \, dS, \end{aligned} \quad (14)$$

respectively with  $p, q = 1, \dots, N_h$ . Formally, from (13), one derives

$$\mathbf{c} = (\mathbf{A} - k_0^2 \mathbf{B})^{-1} \mathbf{d},$$

so that the pressure field is obtained from (12) as

$$\tilde{\psi}_F(x, y, z) = \sum_{q=1}^{N_h} c_q(F) \psi_q(x, y, z), \quad (15)$$

where we have highlighted the dependence of  $\tilde{\psi}$  and of the coefficients  $c_q$  on the boundary data  $F$ , by generalizing notation in (12).

## 4 A reduced finite element formulation

We are now ready to introduce the new discretization based on the HiMod reduction. This discretization relies on choosing the discrete shape and test functions in a form tailored to the problem at hand. In particular, the intrinsic directionality of the pipeline  $\Omega$  justifies the splitting of the dependence of both the shape and the test functions on the spatial variables,  $x$ ,  $y$ , and  $z$ , in the spirit of a separation of variables. Since  $z$  is the leading direction, in accordance with [9, 10, 11, 24, 15, 25], we adopt the hierarchical modal representation

$$\psi_q(x, y, z) = \phi_{n(i)}(x, y)g_j(z), \quad (16)$$

for functions  $\psi_q$  in  $\mathcal{B}$ , where  $\phi_{n(i)}(x, y)$  denotes a modal function defined on the circular cross-section of the tube with hard boundary conditions (see Appendix B for the detailed expression), while  $g_j(z)$  is a 1D shape function associated with the leading direction  $z$ . From (16), the HiMod reduced approximation for the pressure field becomes

$$\tilde{\psi}(x, y, z) = \sum_{i=1}^M \sum_{j=1}^{n_h} \tilde{c}_{i,j} \phi_{n(i)}(x, y)g_j(z), \quad (17)$$

with  $M$  the modal index,  $n_h$  the dimension of the discrete space adopted to approximate the main direction, and where a correspondence between indices  $i$ ,  $n(i)$  and  $j$  is established according to the discretization selected along the different directions (see, e.g., [16, 17, 8]). In (17), the set  $\{\tilde{c}_{i,j}\}_{i=1,j=1}^{M,n_h} \subset \mathbb{C}$  collects the so-called modal coefficients, which represent the actual unknowns of the HiMod discretization. Moreover, we introduce the set  $\mathcal{M} = \{\phi_{n(i)}\}_{i=1}^M$  of the modal basis functions used to model the transverse dynamics, and the basis,  $\mathcal{B}_{1D} = \{g_j\}_{j=1}^{n_h}$ , characterizing the approximation adopted along the mainstream. In particular, functions in  $\mathcal{M}$  are assumed to be  $L^2$ -orthogonal on the circular cross-section. In the numerical validation of Section 6, we resort to a standard continuous FE discretization along  $z$ , so that functions  $g_j$  coincide with piecewise polynomials of arbitrary degree, while we employ modal functions strictly customized to the problem at hand, i.e., coinciding with the eigenfunctions of the Helmholtz equation solved in a circle of radius  $R$  and completed by hard homogeneous Neumann boundary conditions. Completeness of eigenfunctions ensures the possibility to represent arbitrary transverse dynamics with a weighted sum of modal functions. The advantages expected from representation (17) have been successfully investigated in other applicative contexts such as, for instance, in hemodynamic modeling [8]. In particular, since we are mainly interested in small deformations, we do expect that only few modes have to be adopted to represent the scattering problem, corresponding to all propagating modes in the bandwidth of interest plus a few evanescent modes. This should lead to a considerable reduction in terms of number of dofs required to accurately model the pressure  $\psi$  in (11).

Now, to provide the HiMod reduced formulation for problem (11), we exploit the modal representation (17) for the pressure and we choose the test function as  $\varphi = \varphi(x, y, z) = \phi_{n(s)}(x, y)g_t(z)$ , for  $s = 1, \dots, M$ ,  $t = 1, \dots, n_h$ . After moving to polar

coordinates, the arrays in (14) are replaced by the reduced quantities

$$\begin{aligned}
\mathbf{A}_{st,ij}^R &= \\
&\int_0^L g_j(z) g_t(z) \left( \int_0^{2\pi} \int_0^R \nabla_\tau \phi_{n(i)}(\rho, \theta) \cdot \overline{\overline{T}}_{\tau\tau}(\rho, \theta, z) \nabla_\tau \phi_{n(s)}(\rho, \theta) \rho d\rho d\theta \right) dz \\
&+ \int_0^L \frac{dg_j(z)}{dz} g_t(z) \left( \int_0^{2\pi} \int_0^R \phi_{n(i)}(\rho, \theta) \mathbf{i}_z \cdot \overline{\overline{T}}_{z\tau}(\rho, \theta, z) \nabla_\tau \phi_{n(s)}(\rho, \theta) \rho d\rho d\theta \right) dz \\
&+ \int_0^L g_j(z) \frac{dg_t(z)}{dz} \left( \int_0^{2\pi} \int_0^R \nabla_\tau \phi_{n(i)}(\rho, \theta) \cdot \overline{\overline{T}}_{\tau z}(\rho, \theta, z) \mathbf{i}_z \phi_{n(s)}(\rho, \theta) \rho d\rho d\theta \right) dz \\
&+ \int_0^L \frac{dg_j(z)}{dz} \frac{dg_t(z)}{dz} \left( \int_0^{2\pi} \int_0^R \phi_{n(i)}(\rho, \theta) \mathbf{i}_z \cdot \overline{\overline{T}}_{zz}(\rho, \theta, z) \mathbf{i}_z \phi_{n(s)}(\rho, \theta) \rho d\rho d\theta \right) dz, \\
\mathbf{B}_{st,ij}^R &= \int_0^L g_j(z) g_t(z) \left( \int_0^{2\pi} \int_0^R \frac{\phi_{n(i)}(\rho, \theta) \phi_{n(s)}(\rho, \theta)}{\det(\overline{\overline{J}}(\rho, \theta, z))} \rho d\rho d\theta \right) dz, \\
\mathbf{c}_{ij,1}^R &= \tilde{c}_{i,j}, \\
\mathbf{d}_{st,1}^R &= \int_0^{2\pi} \int_0^R \phi_{n(s)}(\rho, \theta) g_t(z_T) \phi_{Tm}(\rho, \theta) \rho d\rho d\theta,
\end{aligned} \tag{18}$$

with  $i, s = 1, \dots, M$ ,  $j, t = 1, \dots, n_h$ ;  $\mathbf{i}_z$  the unit vector associated with the  $z$ -axis;  $\nabla_\tau$  the gradient over the cross-section transverse to  $z$ ;  $\overline{\overline{T}}_{\beta\delta}$  the generic component of the constitutive tensor  $\overline{\overline{T}}$ , for  $\beta, \delta = \tau, z$  (we refer to Appendix A for more details about tensors' components).

Notice that the source term  $F = F(x, y, z)$  in (14) here coincides with one of the acoustic modes at the input/output ports, i.e., with one of the modal functions,  $\phi_{Tm}$ , switched on at the generic pipe's port,  $T$ , located at  $z = z_T$ , with  $m = 1, \dots, N$ . Moreover, since we adopt the same number of modes along the whole pipe according to a uniform HiMod reduction [24, 25], it turns out that  $N = M$ .

The orthogonality of the modal functions ensures that the integral in the definition of vector  $\mathbf{d}_{st,1}^R$  is non-zero only when function  $\phi_{n(s)}$  is non-zero at the generic port  $T$ , namely when  $n(s) = Tm$ .

Functions  $\phi_{Tm}$  will constitute the basis of modal functions,  $\phi_{n(i)}$ , adopted in (17) for the HiMod approximation. The same notation will be adopted to denote the modal functions both when referring to Cartesian and polar coordinates.

Finally, from a computational viewpoint, matrices  $\mathbf{A}^R$  and  $\mathbf{B}^R$  belong to  $\mathbb{R}^{Mn_h \times Mn_h}$ , while vectors  $\mathbf{c}^R, \mathbf{d}^R \in \mathbb{C}^{Mn_h}$ . This means that, if  $M$  is small enough, we are dealing with a linear system characterized by a dimension considerably lower compared with the one of system (13). Actually, after precomputing the modal functions in  $\mathcal{M}$ , the HiMod discretization allows us to replace the 3D full system in (13) with a system of  $M$  coupled 1D problems defined along  $z$ . This leads to a considerable computational saving and to relevant methodological simplifications. For instance, the spatial discretization now involved concerns the centerline of the pipe (i.e., a 1D domain) instead of the whole pipe (i.e., a 3D domain).

## 5 Multimodal Acoustic Impedance and Scattering matrices

In order to provide a complete description of the scattering problem in the deformed pipeline, we resort to the multimodal scattering matrix,  $\mathbf{S}$ . Indeed, this matrix models the set of all scattered modal waves induced by all the possible incident modal waves, when applied one at a time [26]. Since the two ports characterizing the pipeline are equal-sized, we can adopt the same set of modal functions to model the corresponding acoustic modes. In order to compute the scattering matrix, we introduce the multimodal acoustic impedance matrix,  $\mathbf{Z}$ ,  $\mathbf{S}$  being computable from  $\mathbf{Z}$  by simple algebra. Since we have two ports, we can split matrix  $\mathbf{Z}$  into a 2-by-2 block matrix, i.e., as

$$\mathbf{Z} = \begin{bmatrix} \mathbf{Z}_{11} & \mathbf{Z}_{12} \\ \mathbf{Z}_{21} & \mathbf{Z}_{22} \end{bmatrix}, \quad (19)$$

where the subscripts refer to ports, after labeling ports by 1 and 2. The generic block  $\mathbf{Z}_{PQ}$ , is defined by

$$[\mathbf{Z}_{PQ}]_{m,n} = j\omega\varrho_0 \int_{\partial\Omega_P} \phi_{Pm}(\rho, \theta) \tilde{\psi}_{Qn}(\rho, \theta, z_P) \rho d\rho d\theta, \quad (20)$$

with  $P, Q = 1, 2$  and  $m, n = 1, \dots, N$ , where, according to the notation in (17),  $\tilde{\psi}_{Qn}(\rho, \theta, z)$  denotes the HiMod pressure field induced by the impulse  $F = \phi_{Qn}$  at the port  $Q$  and  $F = 0$  elsewhere, measured on the portion,  $\partial\Omega_P = [0, R] \times [0, 2\pi] \times \{z_P\}$ , of  $\partial\Omega$  relative to port  $P$ ,  $\phi_{Qn}$  and  $\phi_{Pm}$  being defined as in (18). This corresponds to applying a hard boundary condition on  $\partial\Omega \setminus \partial\Omega_Q$ .

In order to introduce the multimodal scattering matrix  $\mathbf{S}$ , we first consider a modal expansion of the acoustic pressure field,  $\phi_T$ , and of the normal speed,  $v_T$ , at the generic port  $T$ , with  $T = 1, 2$ , in the form

$$\begin{aligned} \phi_T(x, y) &= \sum_{m=1}^N (A_{Tm}^+ + A_{Tm}^-) \phi_{Tm}(x, y), \\ v_T(x, y) &= \sum_{m=1}^N \frac{\gamma_{Tm}}{j\omega\varrho_0} (A_{Tm}^+ - A_{Tm}^-) \phi_{Tm}(x, y), \end{aligned} \quad (21)$$

where  $N$  is the number of the incident modal waves,  $\gamma_{Tm}$  denotes the propagation constant,  $A_{Tm}^+$  ( $A_{Tm}^-$ ) is an amplitude coefficient characterizing the wave traveling in the positive (negative) direction along the  $z$ -axis induced by the  $m$ -th mode at port  $T$ , while  $\phi_{Tm}$  denotes the corresponding mode eigenfunction (we refer to Appendix B for the explicit definition of both  $\gamma_{Tm}$  and  $\phi_{Tm}$ ). We remark that, hereafter, notation  $\phi_{Tm}$  refers to modal eigenfunctions in a normalized form (see (25)). In deriving the expression for  $v_T$  in (21), we used relation (1) and the fact that modal waves behave as  $\exp(-\gamma_{Tm}z)$  and as  $\exp(\gamma_{Tm}z)$  for the waves travelling along the positive and the negative  $z$ -direction, respectively.

Now, the multimodal scattering matrix  $S$  can be defined by inheriting the splitting of matrix  $\mathbf{Z}$ , i.e., as

$$\mathbf{S} = \begin{bmatrix} \mathbf{S}_{11} & \mathbf{S}_{12} \\ \mathbf{S}_{21} & \mathbf{S}_{22} \end{bmatrix}, \quad (22)$$

where, after labeling ports by 1 and by 2 as in (19), the four blocks  $\mathbf{S}_{PQ} \in \mathbb{C}^{N \times N}$ , with  $P, Q = 1, 2$ , are defined by

$$\begin{aligned} [\mathbf{S}_{11}]_{m,n} &= \frac{A_{1m}^-}{A_{1n}^+} \Big|_{A_{1l}^+ = 0 (l \neq n), A_{2l}^- = 0} \\ [\mathbf{S}_{12}]_{m,n} &= \frac{A_{1m}^-}{A_{2n}^-} \Big|_{A_{2l}^- = 0 (l \neq n), A_{1l}^+ = 0} \\ [\mathbf{S}_{21}]_{m,n} &= \frac{A_{2m}^+}{A_{1n}^+} \Big|_{A_{1l}^+ = 0 (l \neq n), A_{2l}^- = 0} \\ [\mathbf{S}_{22}]_{m,n} &= \frac{A_{2m}^+}{A_{2n}^-} \Big|_{A_{2l}^- = 0 (l \neq n), A_{1l}^+ = 0} \end{aligned} \quad (23)$$

for  $m, n, l = 1, \dots, N$  [27]. Modal eigenfunctions,  $\phi_{Tm}$ , are normalized, so that they can be identified with “power” waves. Actually, for each mode, the average traveling power is half the integral, over the port cross section  $\partial\Omega_T = [0, R] \times [0, 2\pi] \times \{z_T\}$ , of the product between the pressure,  $\phi_T$ , and the conjugate of the particle speed,  $v_T$ , in the  $z$ -direction. More specifically, we have that the power  $W_{Tm}^+$  ( $W_{Tm}^-$ ) travelling in the positive (negative)  $z$ -direction is

$$W_{Tm}^\pm = \mp \frac{1}{2} \frac{\gamma_{Tm}^*}{j\omega\varrho_0} |A_{Tm}^\pm|^2 \int_{\partial\Omega_T} |\phi_{Tm}|^2 dS, \quad (24)$$

with  $\gamma_{Tm}^*$  the conjugate complex of  $\gamma_{Tm}$ . In particular, the normalization of the modal eigenfunctions is chosen such that

$$W_{Tm}^\pm = \mp \frac{1}{2} |A_{Tm}^\pm|^2, \quad (25)$$

so that  $|[\mathbf{S}_{PQ}]_{m,n}|^2$ , for  $P, Q = 1, 2$  and  $m, n = 1, \dots, N$ , represents a relative scattered power (for propagating waves). After introducing vectors

$$\mathbf{A}_T^\pm = [A_{T1}^\pm, A_{T2}^\pm \dots A_{TN}^\pm]^T$$

with  $T = 1, 2$ , thanks to the normalization (25), we have that the multimode impedance matrix,  $\mathbf{Z}$ , characterizes the following relationship

$$\begin{bmatrix} \mathbf{A}_1^+ + \mathbf{A}_1^- \\ \mathbf{A}_2^+ + \mathbf{A}_2^- \end{bmatrix} = \mathbf{Z} \begin{bmatrix} \mathbf{A}_1^+ - \mathbf{A}_1^- \\ \mathbf{A}_2^+ - \mathbf{A}_2^- \end{bmatrix}, \quad (26)$$

while the multimodal scattering matrix,  $\mathbf{S}$ , is associated with the equality

$$\begin{bmatrix} \mathbf{A}_1^- \\ \mathbf{A}_2^- \end{bmatrix} = \mathbf{S} \begin{bmatrix} \mathbf{A}_1^+ \\ \mathbf{A}_2^+ \end{bmatrix}. \quad (27)$$

Simple algebraic manipulations yield the final result

$$\mathbf{S} = (\mathbf{Z} + \mathbf{I})^{-1}(\mathbf{Z} - \mathbf{I}),$$

with  $\mathbf{I} \in \mathbb{R}^{2N \times 2N}$  the identity matrix [27].

The multimodal scattering matrix constitutes what is demanded to implement reflectometric techniques, since these are based on the evaluation of scattering amplitudes and phases as a function of frequency. In the following section, we demonstrate the outstanding performance of HiMod in the computation of  $\mathbf{S}$  by comparing the results obtained against a standard FE analysis carried out by a well known commercial software, both in terms of accuracy and CPU time.

## 6 Numerical results

The verification of the effectiveness of the reduced modeling technique proposed in this paper is carried out on two test cases. In particular, we compare the HiMod discretization with a full 3D FE solution obtained by using the commercial software Comsol Multiphysics<sup>TM</sup> [28]. The normalization used for the scattering matrix in Comsol Multiphysics is different with respect to the one we have adopted in (25). In particular, in Comsol Multiphysics the scattering coefficients are such that each modal function has a maximum value equal to one. Therefore, the generic scattering coefficient provided by Comsol Multiphysics is a ratio between maximum pressure values for modal waves. Thus, to perform a fair comparison between the reduced and the full models, we resort to a renormalization of the scattering matrix computed by Comsol Multiphysics in order to comply with the power wave definition in (24)-(25). In both the examples, we consider waves propagating in the air, with a sound speed value  $v_0 = \sqrt{b_0/\varrho_0} = 343$  m/s, and a rest density  $\varrho_0 = 1.1824$  kg/m<sup>3</sup>.

### 6.1 Test case 1: boundary reduction

The first example consists of a mild deformation of sinusoidal shape for a pipeline of length  $L = 6$  m. The deformation corresponds to a boundary size reduction together with a deviation from the circular shape. The input and output pipeline cross-sections have radius  $R = 0.25$  m. We adopt such a value as the constant radius mapping the original geometry into the reference one via the HiMod map. The boundary of the deformed pipe is described by function

$$\tilde{\rho}'(\theta', z') = R - 0.5^2 R \left( \cos \left( \frac{2\pi z'}{L} \right) + 1 \right) \sin \left( \frac{\theta'}{2} \right), \quad (28)$$

with  $-L/2 \leq z' \leq L/2$ . Actually, equation (28) represents a sinusoidal deformation along the  $z'$  direction, whose amplitude depends on  $\theta'$  and attains its minimum at  $\theta' = \pi$ . On the contrary, for  $\theta' = 0$ , there is no deformation. A plot of the resulting tube is shown in Figure 2 (a).

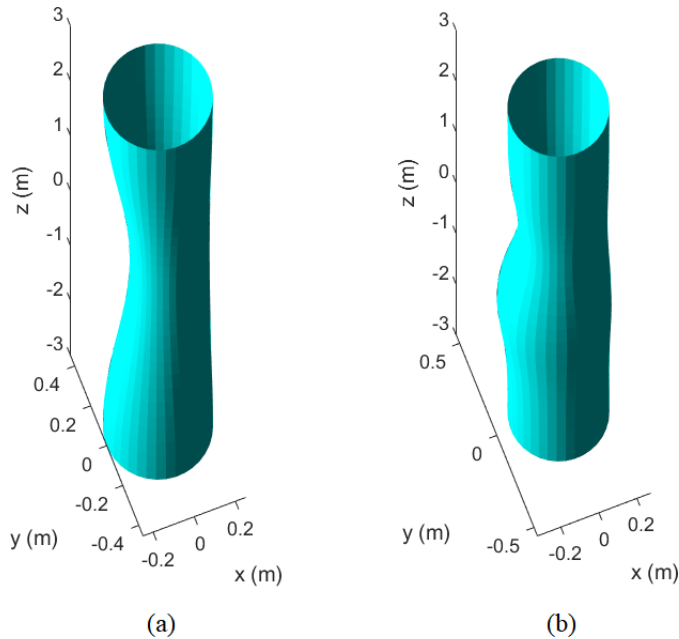


Figure 2: (a) Test case 1: pipeline with the deformation described by (28). (b) Test case 2: pipeline with the deformation described by (29).

For  $R = 0.25$  m, the first higher-order mode has a cutoff frequency of about 402 Hz. At 1000 Hz, there are 8 modes in propagation and since we wish to extend the investigation up to 1000 Hz, we use 10 modes at each port in the analysis in (21) (i.e., we set  $N = 10$ ), and we resort to 10 transverse functions  $\phi_{n(i)}$  to select the reduced model in (17) (i.e., we pick  $M = 10$ ). The total number of dofs also depends on the discretization adopted along the  $z$ -coordinate. We employ quadratic FE associated with a partition of the supporting fiber into subintervals with a maximum length equal to  $\lambda_{\min}/10$ , with  $\lambda_{\min} \simeq 34$  cm. Therefore, the total number of dofs is equal to about 4000.

We have analyzed the same configuration in Comsol Multiphysics by means of a full 3D FE model with quadratic elements, and by using two different meshes, a coarse one characterized by 32622 dofs and a fine one with 247616 dofs.

The comparison between the full and the reduced models is performed in terms of the scattering parameter  $S_{ij}$ , which represents the reflection of mode  $i$  at port 1 when mode  $j$  is incident at port 1 too (we refer to Appendix B for an explicit definition of the modes). With reference to definition (23), parameter  $S_{ij}$  does coincide with  $[\mathbf{S}_{11}]_{i,j}$  with  $i, j = 1, \dots, 10$ . In Figure 3, we show the magnitude of four parameters  $S_{ij}$ , expressed in dB, as a function of the frequency both for the full and the HiMod models. Moreover, in Table 1, we collect the CPU time per frequency point needed for the analysis, to have a comparison also in terms of modeling efficiency.<sup>1</sup>

It is evident a very good matching between the full solution provided by Comsol Multi-

<sup>1</sup>All CPU times refer to an Intel i7 processor with 3 GHz clock rate.

physics on the fine mesh and the HiMod discretization for almost all scattering parameters, up to the maximum frequency. On the contrary, as expected, Comsol Multiphysics does not yield reliable values when run on the coarse mesh, especially as frequency increases. Parameter  $S_{31}$  is the one less sharply detected by HiMod. Ideally, this coefficient should be equal to  $-\infty$  dB, because the mode is not excited by the deformation. The oscillations in the plot coincide with numerical noise due to the selected mesh and discretization. In particular, the HiMod procedure exhibits some noise in the range 400–700 Hz, corresponding to the onset of mode 2 and 3 (402 Hz). Concerning the Comsol Multiphysics approximation, we obtain an increasing value of the scattering coefficient when using a fine mesh. This suggests employing an even finer mesh to reduce the noise, with an unavoidable boosting of the CPU time.

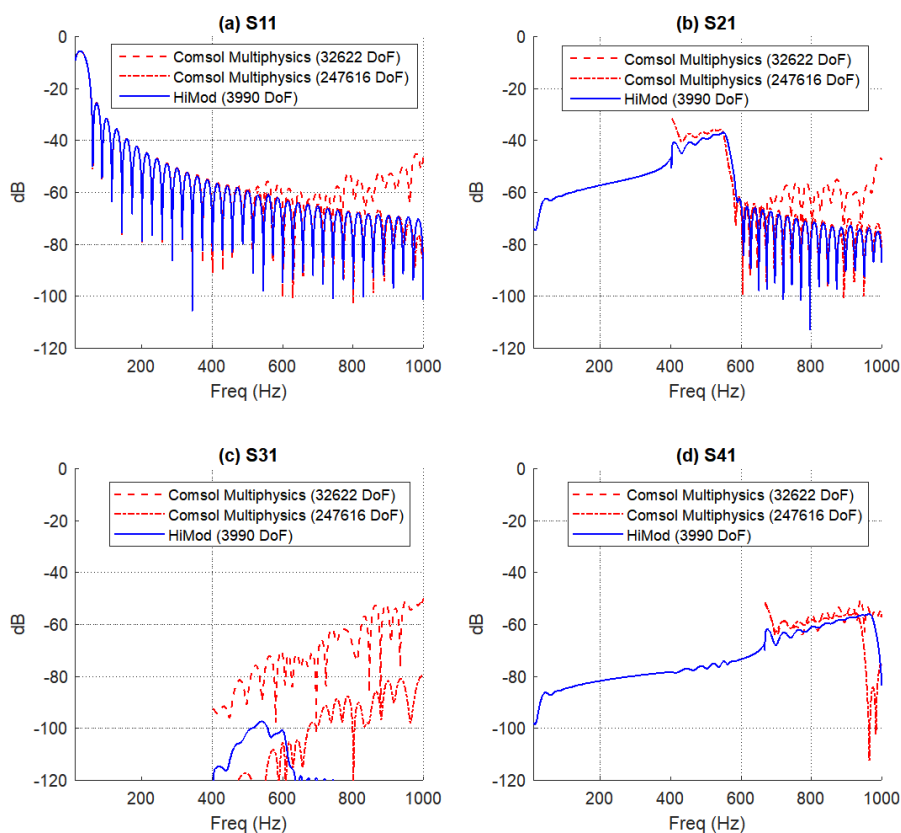


Figure 3: Test case 1. Trend of the parameters  $S_{i1}$ , for  $i = 1, \dots, 4$ , as function of the frequency, when mode 1 is incident: comparison between Comsol Multiphysics, for two different choices of the mesh, and the HiMod approach.

As far as the CPU time is concerned, there is a considerable discrepancy between full and reduced order models, even when dealing with the coarse mesh. In this last case, the time required by Comsol Multiphysics is about 15 times larger than that demanded by HiMod. This gap increases to 200 times when computing the full model on the fine

Table 1: Test case 1. Performance comparison between full and HiMod models.

Software	dofs	CPU time
Comsol Multiphysics <sup>TM</sup> coarse mesh	32622	0.75 sec/freq
Comsol Multiphysics <sup>TM</sup> dense mesh	247616	9.5 sec/freq
HiMod (this work)	4000	0.05 sec/freq

mesh (see Table 1).

## 6.2 Test case 2: boundary reduction and enlargement

As a second configuration, we consider a deformation that induces both a size reduction and a size enlargement along the pipe. Using the same input/output radius as in the previous test case ( $R = 0.25$  m), we can characterize the boundary of the pipe by the equation

$$\tilde{\rho}'(\theta', z') = R - 0.5 R z' \exp \left[ - \left( \frac{6z'}{L} \right)^2 \right] \sin \left( \frac{\theta'}{2} \right), \quad (29)$$

with  $-L/2 \leq z' \leq L/2$  and  $L = 6$ . A plot of the pipe is shown in Figure 2 (b). As for Test case 1, we adopt as a reference solution the quadratic FE approximation provided by Comsol Multiphysics on two different meshes, now consisting of 29983 (coarse mesh) and 296906 (dense mesh) dofs, respectively.

We replicate the investigation performed in Section 6.1, by considering the accuracy and the efficiency of the HiMod reduction when computing the scattering parameters  $S_{ij}$ . The results of such an analysis are presented in Figure 4. Also for this case, we summarize the performances in terms of CPU time in Table 2.

We can draw conclusions very similar to the ones for Test case 1. The Comsol Multiphysics solution computed on the coarse mesh predicts a trend for parameters  $S_{ij}$  which is not reliable for high frequencies. On the other hand, the Comsol Multiphysics model associated with the fine mesh and the HiMod approximation provide a fully comparable trend for indices  $S_{11}$ ,  $S_{21}$ ,  $S_{41}$ , while still exhibiting a certain mismatch in the modeling of  $S_{31}$ . As for the previous case, mode 3 is not excited by the deformation. As a consequence, the non-zero values in the figure can be ascribed to numerical noise. Only close to the cutoff of modes 2 and 3, we recognize an increment of the numerical noise when using the HiMod method, whereas, by using Comsol Multiphysics, the noise increases constantly with frequency, up to  $-80$  dB at 1000 Hz. This suggests that a finer mesh is required to guarantee a more accurate analysis in the higher part of the spectrum.

The values for the CPU time in Table 2 confirm the high efficiency of the HiMod reduction procedure, which is about 14 and 200 times faster with respect to the performances of the Comsol Multiphysics model when using the coarse and the fine mesh, respectively.

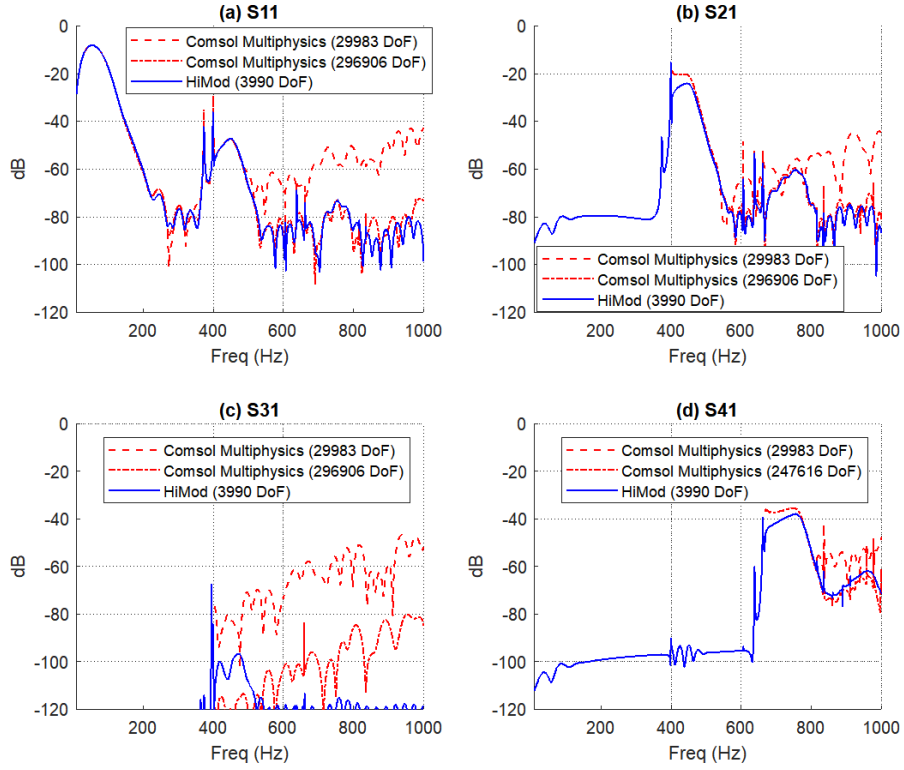


Figure 4: Test case 2. Trend of the parameters  $S_{i1}$ , for  $i = 1, \dots, 4$ , as function of the frequency, when mode 1 is incident: comparison between Cmsol Multiphysics, for two different choices of the mesh, and the HiMod approach.

Table 2: Test case 2. Performance comparison between full and HiMod models

Software	dofs	CPU time
Cmsol Multiphysics <sup>TM</sup> coarse mesh	29983	0.7 sec/freq
Cmsol Multiphysics <sup>TM</sup> dense mesh	296906	11.6 sec/freq
HiMod (this work)	4000	0.05 sec/freq

## 7 Conclusions and future developments

We discussed the application of the HiMod discretization to the linearized acoustic problem. So far, this model reduction technique has been successfully employed for the blood flow simulation. This paper provides a first attempt to employ the same procedure in a different applicative context. The adoption of a customized modal basis of functions as well as the definition of the HiMod map changing the physical domain into the reference one represent the key steps for a HiMod reduction. As a consequence, these two issues have been thoroughly investigated in the paper.

Numerical verification shows that the multimode acoustic scattering matrix can be accurately computed by HiMod, with a speed-up factor of about 200 when compared with a well-established 3D FE solver such as Comsol Multiphysics. These computational advantages become more and more relevant as the number of the dofs increases. As an additional check to the test cases here included, we managed to solve a 100 m long pipeline on a standard PC with 16 GB RAM, without resorting to special techniques. The same problem tackled with a 3D FE analysis would require hardware resources well beyond the ones of a common laptop.

Several extensions of the current analysis can be itemized. Among the possible future developments, we cite the interest for a parametric setting. Actually, parametric problems play a crucial role when dealing with multi-query contexts, such as optimization loops or uncertainty quantification. A priori, parameters may coincide with any problem data. A case of particular interest is represented by the parametrization of the geometry. In [29, 30, 31], two different parametric counterparts of HiMod reduction are provided. These works will provide us with the reference background to generalize the present modeling to more challenging acoustic configurations.

Non-linear unsteady problems represent another issue of relevant interest with a view to real-life simulations. A first attempt to formalize the time-dependent version of the HiMod discretization is presented and numerically checked in [32].

## A The HiMod map

In this appendix, we detail the transformation adopted in Section 2 to commute the physical domain,  $\Omega'$ , into the reference one,  $\Omega$ , (see Figure 1). The pipeline boundary,  $\partial\Omega'$ , is described by a radial distance from the  $z'$ -axis coinciding with a function,  $\tilde{\rho}'(\theta', z')$ , of  $\theta'$  and  $z'$ . We assume that the  $z'$ -coordinate is sampled with  $N_z$  points and, for each sampled coordinate, we consider a pipeline cross-section, defined by  $N_b$  points. We use index  $k$  to label the sampled  $z'$ -coordinate and index  $r$  to denote the points discretizing (counterclockwise) the boundary of the  $k$ -th cross-section, so that the  $k$ -th pipeline section is identified by the pairs  $(\tilde{x}'_{r,k}, \tilde{y}'_{r,k})$  in Cartesian coordinates or, likewise, by  $(\tilde{\rho}'_{r,k}, \tilde{\theta}'_{r,k})$  in polar coordinates, with  $r = 1, \dots, N_b$ ,  $k = 1, \dots, N_z$ . In Figure 5, we show a schematization of the geometric parameters.

The HiMod map that we adopt converts each cross-section of  $\Omega'$  to a circle of radius  $R$ . The boundary of the  $k$ -th cross-section is described in polar coordinates through a

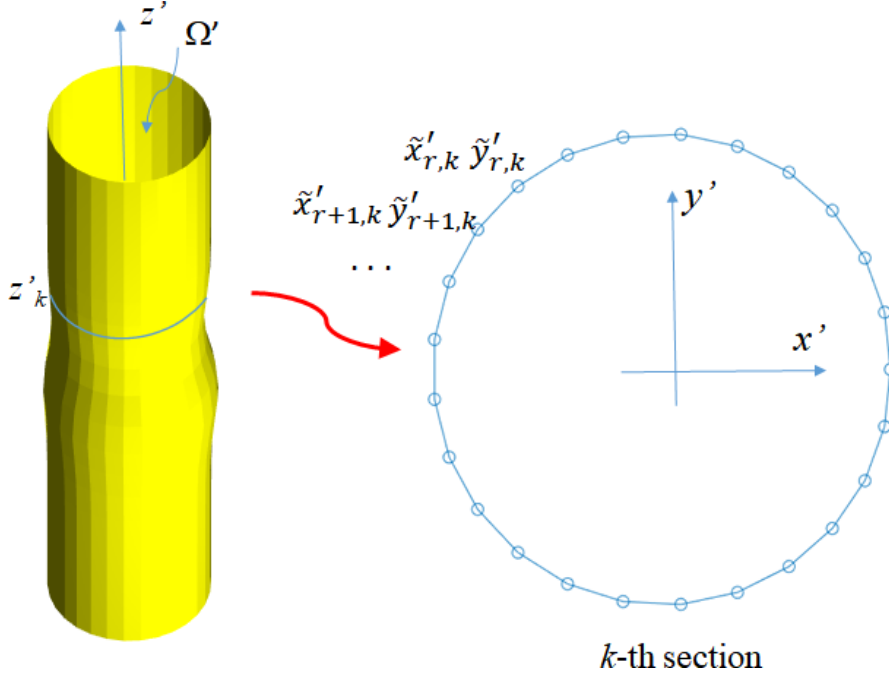


Figure 5:  $k$ -th section of the pipeline: the points along the boundary of the cross-section are labeled counterclockwise by index  $r$ .

piecewise linear interpolation, so that

$$\tilde{\rho}'_k(\theta') = \tilde{\rho}'_{r,k} \frac{(\tilde{\theta}'_{r+1,k} - \theta')}{\Delta_{\theta,r}} + \tilde{\rho}'_{r+1,k} \frac{(\theta' - \tilde{\theta}'_{r,k})}{\Delta_{\theta,r}} \quad \text{for } \theta' \in [\tilde{\theta}'_{r,k}, \tilde{\theta}'_{r+1,k}],$$

with  $\Delta_{\theta,r} = \tilde{\theta}'_{r+1,k} - \tilde{\theta}'_{r,k}$  the discrete angular step and  $r = 1, \dots, N_b - 1$ .

Consider now the volume of the pipeline in the slab  $z'_k \leq z' \leq z'_{k+1}$ . Then, each point  $P'(\rho', \theta', z') \in \Omega'$  is mapped into a point  $P(\rho, \theta, z) \in \Omega$  by the map

$$\begin{cases} \rho = \rho' \frac{R}{\tilde{\rho}'_k(\theta') Z_k + \tilde{\rho}'_{k+1}(\theta') Z_{k+1}} \\ \theta = \theta' \\ z = z', \end{cases} \quad (30)$$

with  $Z_k = (z_{k+1} - z)/\Delta_{z,k}$ ,  $Z_{k+1} = (z - z_k)/\Delta_{z,k}$  and  $\Delta_{z,k} = z_{k+1} - z_k$ . Note that transformation (30) defines a linear interpolation between  $\tilde{\rho}'_k$  and  $\tilde{\rho}'_{k+1}$  along the  $z$ -direction.

A more straightforward derivation can be obtained with the inverse transformation of

the map in (30), given by

$$\begin{cases} \rho' = \rho \frac{\tilde{\rho}'_k(\theta)Z_k + \tilde{\rho}'_{k+1}(\theta)Z_{k+1}}{R} \\ \theta' = \theta \\ z' = z, \end{cases}$$

for  $z_k \leq z \leq z_{k+1}$ , whose Jacobian, in Cartesian coordinates, coincides with

$$\overline{\overline{J}}' = \overline{\overline{J}}'(x, y, z) = \begin{bmatrix} \frac{\partial x'}{\partial x} & \frac{\partial x'}{\partial y} & \frac{\partial x'}{\partial z} \\ \frac{\partial y'}{\partial x} & \frac{\partial y'}{\partial y} & \frac{\partial y'}{\partial z} \\ 0 & 0 & 1 \end{bmatrix} = \overline{\overline{J}}^{-1},$$

with  $\overline{\overline{J}}$  the matrix defined in (7), whereas, in polar coordinates, we have

$$\overline{\overline{J}}' = \overline{\overline{J}}'(\rho, \theta, z) = \begin{bmatrix} \cos \theta & -\sin \theta & 0 \\ \sin \theta & \cos \theta & 0 \\ 0 & 0 & 1 \end{bmatrix} \begin{bmatrix} \frac{\partial \rho'}{\partial \rho} & \frac{\partial \rho'}{\rho \partial \theta} & \frac{\partial \rho'}{\partial z} \\ 0 & \frac{\rho'}{\rho} & 0 \\ 0 & 0 & 1 \end{bmatrix} \begin{bmatrix} \cos \theta & \sin \theta & 0 \\ -\sin \theta & \cos \theta & 0 \\ 0 & 0 & 1 \end{bmatrix},$$

where

$$\begin{cases} \frac{\partial \rho'}{\partial \rho} = \frac{\tilde{\rho}'_k(\theta)Z_k + \tilde{\rho}'_{k+1}(\theta)Z_{k+1}}{R} \\ \frac{\partial \rho'}{\rho \partial \theta} = \frac{\tilde{\rho}'_{r+1,k} - \tilde{\rho}'_{r,k}}{R\Delta_{\theta,k}}Z_k + \frac{\tilde{\rho}'_{r+1,k+1} - \tilde{\rho}'_{r,k+1}}{R\Delta_{\theta,k+1}}Z_{k+1} \\ \frac{\partial \rho'}{\partial z} = \rho \frac{\tilde{\rho}'_{k+1}(\theta) - \tilde{\rho}'_k(\theta)}{R\Delta_{z,k}} \\ \frac{\rho'}{\rho} = \frac{\tilde{\rho}'_k(\theta)Z_k + \tilde{\rho}'_{k+1}(\theta)Z_{k+1}}{R} \end{cases} \quad (31)$$

for  $z_k \leq z \leq z_{k+1}$ . Relations (31) define the anisotropic material density in the pipeline and allow us to express the Jacobian  $\det(\overline{\overline{J}})$  in (18) in a closed form. In particular, it holds

$$\begin{cases} \overline{\overline{J}}_{\tau\tau} = \mathbf{i}_\rho \mathbf{i}_\rho^T J_{\rho\rho} + \mathbf{i}_\rho \mathbf{i}_\theta^T J_{\rho\theta} + \mathbf{i}_\theta \mathbf{i}_\rho^T J_{\theta\rho} + \mathbf{i}_\theta \mathbf{i}_\theta^T J_{\theta\theta} \\ \overline{\overline{J}}_{\tau z} = \mathbf{i}_\rho \mathbf{i}_z^T J_{\rho z} + \mathbf{i}_\theta \mathbf{i}_z^T J_{\theta z} \\ \overline{\overline{J}}_{z\tau} = \mathbf{i}_z \mathbf{i}_\rho^T J_{z\rho} + \mathbf{i}_z \mathbf{i}_\theta^T J_{z\theta} \\ \overline{\overline{J}}_{zz} = \mathbf{i}_z \mathbf{i}_z^T J_{zz} = \mathbf{i}_z \mathbf{i}_z^T, \end{cases}$$

with  $\mathbf{i}_\rho$ ,  $\mathbf{i}_\theta$ , and  $\mathbf{i}_z$  the unit vectors associated with the radial, the angular and the  $z$  coordinates,  $J_{\sigma\nu}$  the Jacobian components with  $\sigma, \nu = \rho, \theta, z$ .

## B Acoustic modal functions in a circular waveguide

We define the acoustic modal functions  $\phi_{n(i)}$  involved in the HiMod expansion (17), endowed with hard boundary conditions. Mode functions are identified with the acoustic modes  $\phi_{Tm}$  introduced in (18), and coincide with the exact solution to the Helmholtz equation solved on the port cross section,  $\partial\Omega_T$ , when completed with homogeneous hard boundary conditions. In particular, the modal functions are power-normalized on the port cross-section,  $\partial\Omega_T$ , so that

$$W_{Tm}^+ = \frac{1}{2} \left[ \frac{\gamma_{Tm}}{j\omega\rho_0} \right]^* \int_{\partial\Omega_T} \phi_{Tm}(\rho, \theta) \phi_{Tm}^*(\rho, \theta) \rho d\rho d\theta = \frac{1}{2} \quad (32)$$

with  $W_{Tm}^+$  the average complex power along the positive  $z$ -direction and  $\phi_{Tm}^*$  the conjugate complex of  $\phi_{Tm}$ .

Mode 1 with hard boundary conditions is a constant function, i.e.,

$$\phi_1(\rho, \theta) = \frac{1}{R} \sqrt{\frac{\rho_0 v_0}{\pi}},$$

with  $R$  the port radius,  $\rho_0$  the rest density and  $v_0 = \sqrt{b_0/\rho_0}$  the speed of sound,  $b_0$  being the compression modulus. Higher order modal functions can be expressed in terms of Bessel functions as

$$\phi_q(\rho, \theta) = C_{\nu\mu} J_\nu \left( \chi_{\nu\mu} \frac{\rho}{R} \right) \begin{cases} \cos(\nu\theta) \\ \sin(\nu\theta), \end{cases} \quad (33)$$

for  $q > 1$ , where  $J_\nu$  is the Bessel function of the first kind and of (integer) order  $\nu$ , while  $\chi_{\nu\mu}$  is the  $\mu$ -th zero of the first derivative of  $J_\nu$  (with  $\nu = \nu(q)$ ,  $\mu = \mu(q)$ ,  $q$  being the modal index) [33]. In (33),  $C_{\nu\mu}$  is a normalizing term that can be expressed as

$$C_{\nu\mu} = \frac{\chi_{\nu\mu}}{R} \left( \frac{\gamma_q}{j\omega\rho_0} \left| \frac{\pi}{\epsilon_{\nu 0}} (\chi_{\nu\mu}^2 - \nu^2) J_\nu^2(\chi_{\nu\mu}) \right| \right)^{-\frac{1}{2}}, \quad (34)$$

where  $\epsilon_{\nu 0} = 1$  for  $\nu = 0$  and  $\epsilon_{\nu 0} = 2$  otherwise,  $j$  is the imaginary unit,  $\gamma_q = \sqrt{(\chi_{\nu\mu}/R)^2 - k_0^2}$  is the complex propagation constant, with  $\omega$  the angular frequency and  $k_0 = \omega/v_0$  the wavenumber. Notice that, in case  $\nu = 0$ , only the cosine function in (33) is used.

From definitions (33)-(34), we have that the first four modal functions used in Figures 3 and 4 are provided by

$$\begin{aligned} \phi_1(\rho, \theta) &= \frac{1}{R} \sqrt{\frac{\rho_0 v_0}{\pi}} \\ \phi_2(\rho, \theta) &= C_{11} J_1 \left( \chi_{11} \frac{\rho}{R} \right) \cos(\theta) \\ \phi_3(\rho, \theta) &= C_{11} J_1 \left( \chi_{11} \frac{\rho}{R} \right) \sin(\theta) \\ \phi_4(\rho, \theta) &= C_{21} J_2 \left( \chi_{21} \frac{\rho}{R} \right) \cos(2\theta), \end{aligned}$$

respectively. Despite the generally poor convergence performance when involved in a modal expansion with respect to other polynomial approximations [17], Bessel's functions can be advantageously employed in the specific case of our interest, since we are mainly interested in small deformations. Moreover, in the limit case of no deformation, the approximation obtained by Bessel's functions in the transverse plane tends to the exact solution. This contributes to reducing the numerical noise and therefore enhancing the system capability to detect extremely small echoes.

## Acknowledgments

S. Perotto acknowledges the European Union's Horizon 2020 research and innovation programme under the Marie Skłodowska-Curie Actions, grant agreement 872442 (ARIA, Accurate Roms for Industrial Applications), and the research project GNCS-INdAM 2020 "Tecniche Numeriche Avanzate per Applicazioni Industriali".

## References

- [1] J. Muggleton, M. Brennan, R. Pinnington, Wavenumber prediction of waves in buried pipes for water leak detection, *J. Sound Vib.* 249 (2002) 934-954.
- [2] J. Ma, M.J.S. Lowe, F. Simonetti, Measurement of the properties of fluids inside pipes using guided longitudinal waves, *IEEE T. Ultrason. Ferr.* 54(3) (2007) 647-658.
- [3] G. Bernasconi, S. Del Giudice, G. Giunta, Pipeline Acoustic Monitoring, Pipeline Technology Conference, Hannover, 2012.
- [4] G. Bernasconi, S. Del Giudice, G. Giunta, F. Dionigi, Advanced pipeline vibroacoustic monitoring, Proceedings of the ASME 2013 Pressure Vessels & Piping Division Conference, July 14-18, 2013, Paris, France, PVP2013-97281, 2013.
- [5] G.A. Russell, E.D. Hjerpe, On the analogy between the one-dimensional acoustic waveguide and the electrical transmission line, *J. Acoust. Soc. Am.* 94 (1993) 583-584.
- [6] P.M. Morse, *Vibration and Sound*, Acoustical Society of America, New York, 229-232, 1976.
- [7] L.L. Thompson, A review of finite-element methods for time-harmonic acoustics, *J. Acoust. Soc. Am.* 20(3) (2006) 1315-1330.
- [8] Y.A. Brandes Costa Barbosa, S. Perotto, Hierarchically reduced models for the Stokes problem in patient-specific artery segments, *Int. J. Comput. Fluid D.* 34(2) (2020) 160-171.
- [9] A. Ern, S. Perotto, A. Veneziani, Hierarchical model reduction for advection-diffusion-reaction problems, in *Numerical Mathematics and Advanced Applications*,

- K. Kunisch, G. Of, O. Steinbach (Eds.), Springer-Verlag, Berlin Heidelberg, 703-710, 2008.
- [10] S. Perotto, A. Ern, A. Veneziani, Hierarchical local model reduction for elliptic problems: a domain decomposition approach, *Multiscale Model. Simul.* 8(4) (2010) 1102-1127.
- [11] S. Perotto, A. Veneziani, Coupled model and grid adaptivity in hierarchical reduction of elliptic problems, *J. Sci. Comput.* 60(3) (2014) 505-536.
- [12] S. Perotto, A. Reali, P. Rusconi, A. Veneziani, HIGAMod: a hierarchical isogeometric approach for model reduction in curved pipes, *Comput. & Fluids* 142 (2017) 21-29.
- [13] S.A. Cummer, D. Schurig, One path to acoustic cloaking, *New J. Phys.* 9(45) 2007.
- [14] G.W. Milton, M. Briane, J.R. Willis, On cloaking for elasticity and physical equations with a transformation invariant form, *New J. Phys.* 8(248) 2006.
- [15] S. Perotto, Hierarchical model (Hi-Mod) reduction in non-rectilinear domains, in *Domain Decomposition Methods in Science and Engineering XXI*, Lect. Notes Comput. Sci. Eng., 98, J. Erhel, M. Gander, L. Halpern, G. Pichot, T. Sassi, O. Widlund (Eds), Springer, Cham, 477-485, 2014.
- [16] M.C. Aletti, S. Perotto, A. Veneziani, HiMod reduction of advection-diffusion-reaction problems with general boundary conditions, *J. Sci. Comput.* 76(1) (2018) 89-119.
- [17] S. Guzzetti, S. Perotto, A. Veneziani, Hierarchical model reduction for incompressible fluids in pipes, *Int. J. Numer. Meth. Eng.* 114(5) (2018) 469-500.
- [18] A.T. Fabro, N.S. Ferguson, B.R. Mace, Wave propagation in slowly varying waveguides using a finite element approach, *J. Sound Vib.* 442 (2019) 308-329.
- [19] Y.-L. Tsai, T. Chen, Transformation media in acoustics with constant bulk modulus or constant density tensor, *J. Mech.* 32(3) (2016) 313-323.
- [20] A.N. Norris, Acoustic Cloaking, *Acoustics Today* 11(1) (2015) 38-46.
- [21] H. Chen, C.T Chan, Acoustic cloaking and transformation acoustics, *J. Phys. D Appl. Phys.* 43 113001 (2010) 1-14.
- [22] S.A Cummer, M. Rahm, D. Schurig, Material parameters and vector scaling in transformation acoustics, *New J. Phys.* 10 115025 (2008).
- [23] A. Ern and J.-L. Guermond, *Theory and Practice of Finite Elements*, Applied Mathematical Sciences 159, Springer-Verlag, New York, 2004.

- [24] S. Perotto, A. Zilio, Hierarchical model reduction: three different approaches, in Numerical Mathematics and Advanced Applications, A. Cangiani, R.L. Davidchack, E. Georgoulis, A.N. Gorbun, J. Levesley, M.V. Tretyakov (Eds.), Springer-Verlag Berlin Heidelberg, 851-859, 2013.
- [25] S. Perotto, A survey of hierarchical model (Hi-Mod) reduction methods for elliptic problems, in Numerical Simulations of Coupled Problems in Engineering, Comput. Methods Appl. Sci., 33, S.R. Idelsohn (Ed.), Springer, Cham, 217-241, 2014.
- [26] A. Reinhardt, T. Pasture, S. Ballandras, V. Laude, Scattering matrix method for acoustic waves in piezoelectric, fluid, and metallic multilayers, J. Appl. Phys. 94(10) (2003) 6923-6931.
- [27] A. Snakowska, K. Kolber, Ł. Gorazd, J. Jurkiewicz, Derivation of an Acoustic Two-Port Scattering Matrix for a Multimode Wave Applying the Single-Mode Generator, 2018 Joint Conference - Acoustics, Ustka, Poland, 1-5, 2018.
- [28] COMSOL Multiphysics<sup>TM</sup> v.5.4. [www.comsol.com](http://www.comsol.com). COMSOL AB, Stockholm, Sweden.
- [29] D. Baroli, C.M. Cova, S. Perotto, L. Sala, A. Veneziani, Hi-POD solution of parametrized fluid dynamics problems: preliminary results, in Model Reduction of Parametrized Systems, MS&A. Model. Simul. Appl., 17 (1017) 235-254.
- [30] M. Lupo Pasini, S. Perotto, Hierarchical model reduction driven by a Proper Orthogonal Decomposition for parametrized advection-diffusion-reaction problems, MOX-Report 60/2020, 2020.
- [31] M. Zancanaro, F. Ballarin, S. Perotto, G. Rozza, Hierarchical model reduction techniques for flow modeling in a parametrized setting, Multiscale Model. Simul. 19(1) (2021) 267-293.
- [32] S. Perotto, A. Zilio, Space-time adaptive hierarchical model reduction for parabolic equations, Adv Model Simul Eng Sci. (2015) 2-25.
- [33] J.P. Boyd, Chebyshev and Fourier Spectral Methods, Dover Publications, New York, 2001.

## MOX Technical Reports, last issues

Dipartimento di Matematica  
Politecnico di Milano, Via Bonardi 9 - 20133 Milano (Italy)

- 43/2021** Salvador, M.; Fedele, M.; Africa, P.C.; Sung, E.; Dede', L.; Prakosa, A.; Chrispin, J.; Trayanov  
*Electromechanical modeling of human ventricles with ischemic cardiomyopathy: numerical simulations in sinus rhythm and under arrhythmia*
- 42/2021** Calissano, A.; Fontana, M.; Zeni, G.; Vantini, S.  
*Conformal Prediction Sets for Populations of Graphs*
- 41/2021** Costa, G., Cavinato, L., Maschi, C., Fiz, F., Sollini, M., Politi, L. S., Chiti, A., Balzarini, L., Ag  
*Virtual Biopsy for Diagnosis of Chemotherapy-Associated Liver Injuries and Steatohepatitis: A Combined Radiomic and Clinical Model in Patients with Colorectal Liver Metastases*
- 40/2021** Martinolli, M.; Cornat, F.; Vergara, C.  
*Computational Fluid-Structure Interaction Study of a new Wave Membrane Blood Pump*
- 39/2021** Barnafi, N.; Di Gregorio, S.; Dede', L.; Zunino, P.; Vergara, C.; Quarteroni, A.  
*A multiscale poromechanics model integrating myocardial perfusion and systemic circulation*
- 37/2021** Dassi, F.; Fumagalli, A.; Mazzieri, I.; Scotti, A.; Vacca, G.  
*A Virtual Element Method for the wave equation on curved edges in two dimensions*
- 36/2021** Parolini, N.; Dede', L.; Antonietti, P. F.; Ardenghi, G.; Manzoni, A.; Miglio, E.; Pugliese, A.; V  
*SUIHTER: A new mathematical model for COVID-19. Application to the analysis of the second epidemic outbreak in Italy*
- 38/2021** Giusteri, G. G.; Miglio, E.; Parolini, N.; Penati, M.; Zambetti, R.  
*Simulation of viscoelastic Cosserat rods based on the geometrically exact dynamics of special Euclidean strands*
- 34/2021** Bonaventura, L.; Gatti F.; Menafoglio A.; Rossi D.; Brambilla D.; Papini M.; Longoni L.  
*An efficient and robust soil erosion model at the basin scale*
- 35/2021** Regazzoni, F.; Quarteroni, A.  
*Accelerating the convergence to a limit cycle in 3D cardiac electromechanical simulations through a data-driven 0D emulator*